Electrical Power and Energy Systems 155 (2024) 109556

Contents lists available at ScienceDirect

International Journal of Electrical Power and Energy Systems

journal homepage: www.elsevier.com/locate/ijepes

Advanced probabilistic load flow methodology for voltage unbalance assessment in PV penetrated distribution grids

Giambattista Gruosso [a,*], Cesar Diaz Londono [a], Luca Daniel [b], Paolo Maffezzoni [a]

[a] Politecnico di Milano, DEIB, Piazza Leonardo da Vinci, 32, Milano, 20135, Italy
[b] MIT, 77 Massachusetts Avenue, Cambridge, 02139, MA, USA

ARTICLE INFO

Keywords:
Data clustering
Multi-variate function approximation
Photovoltaics
Probabilistic load flow
Sensitivity analysis voltage unbalance factor

ABSTRACT

The balancing of three-phase node voltages in modern power distribution grids can be significantly deteriorated by the penetration of single-phase PV renewable sources. For a given grid topology and prescribed loads, voltage unbalance critically depends on the nodes where power is injected. Its amount can vary substantially at different observations Buses in the grid. In this paper, we present a methodology that can inform network operators about the critical Buses in the grid and critical injection scenarios. The method is based on a numerically efficient but accurate probabilistic load flow that can handle the case of many PV sources and provides detailed information on the probability distribution of voltage unbalance. The proposed methodology relies on the complex-domain modeling of voltage unbalance sensitivity and on accelerating Monte Carlo simulations via parameter space partitioning.

1. Introduction

Voltage unbalance is a major power quality concern in modern power distribution grids that can result in a reduction of equipment lifetime and motor efficiency [1,2]. The high penetration of distributed single-phase renewable energy, i.e., Photovoltaic (PV) sources, can significantly aggravate the unbalance problem [3].

Ideally, the assessment of voltage unbalance in PV penetrated power grids would require complete long-time monitoring of voltages at all buses as well as detailed (and in advance) information about all potential PV injection nodes/points and associated power levels. In most practical cases, instead, only limited information about PV deliverable power is available, commonly under the form of historic measurements data-set.

To cope with such an incomplete information, advanced simulation tools capable of predicting in a realistic way the potentially critical scenario and worst case voltage unbalance conditions are of vital importance. From the network operators viewpoint, a first key issue is: *(a) For a given three-phase power distribution grid topology with prescribed nominal loads, simulation tools should identify which Buses are potentially more prone to observe great voltage unbalance due to the penetration of PV sources.*

Voltage unbalance assessment in a PV penetrated grid is complicated by the fact that PV generation is intermittent/uncertain so that grid analysis should be probabilistic, i.e., based on Probabilistic Power Flow (PPF) analysis. A second key feature of advanced simulation tools is: *(b) They should rely on reliable and very efficient probabilistic methods able to explore several critical scenarios with many injection PV sources described by realistic data-based power distributions.*

To this aim, state-of-the art PPF methods can be broadly divided into analytical methods and numerical methods. Analytical methods include cumulant methods [4], point estimate methods [5], and Cornish–Fisher expansion [6]. Such methods are computationally efficient since they provide estimations of uncertain output variables (e.g., node voltages) through a few deterministic formulas. However, in many cases they rely on simplification hypotheses, e.g., they assume that power flow equations are linear over the whole parameters variability space, that do not hold in real system of interest.

Numerical methods are more general and employ sampling techniques and Monte Carlo method (MC). However, due to the slow numerical convergence, the reference MC method involves repeatedly solving an enormous number of power flow problems. As a consequence, the applicability of MC method to distribution grids of practical interest requires the exploitation of proper acceleration techniques. State-of-the-art techniques for MC acceleration include advanced sampling methods [7,8] or rely on surrogate models that approximate the input–output relationships (i.e., between injected power and observe node voltage) determined by the power flow problem [9–12]. Unfortunately, both above-mentioned acceleration approaches lose most of their effectiveness when the number of uncertainty parameters get

* Corresponding author.
E-mail address: giambattista.gruosso@polimi.it (G. Gruosso).

https://doi.org/10.1016/j.ijepes.2023.109556
Received 27 March 2023; Received in revised form 31 August 2023; Accepted 4 October 2023
Available online 14 October 2023

large, (due to the *curse of dimensionality problem*) as it is the case for distribution grids penetrated by many PV sources.

To address such complex scenarios of growing practical interest, in this paper, we present some enhanced simulation tools for voltage unbalance assessment. In doing that, we use the commonly accepted *true definition* of voltage unbalance given by the complex Voltage Unbalance Factor (VUF) [13]. The novel contributions include:

1. A comprehensive sensitivity analysis of complex VUF observable at all Buses in the grid versus all potential power injection nodes. It is worth noticing how several methods for grid sensitivity are available in the literature [14,15]. However, such techniques provide the sensitivity of node voltages magnitude. Extra computation is required to deduce the sensitivity of the non-elementary complex VUF.
2. From VUF sensitivity, some figures of merit coefficients (referred to as β_n, ν_j) are associated to each Bus describing its level of VUF criticality. In fact, Buses with large coefficient values are prone to exhibit great VUF values as well as they tend to induce large VUF in other Buses when are employed as power injection nodes.
3. An advanced probabilistic power flow analysis that is able to accurately and efficiently estimate the variability interval of VUF at critical Buses in grids penetrated by a large number of PV sources. The method employs a parameter space partitioning via a k-means data clustering for overcoming the curse of dimensionality problem. Furthermore, VUF complex sensitivity is exploited to accelerate MC simulations via local approximations of VUF-versus-injected-power relationships.

The remainder of this paper is organized in this way: Section 2 briefly reviews power flow problem formulation. In Section 3, the multi-variate dependence of complex VUF on PV injected powers is formalized, while Section 4 describes VUF sensitivity computation. The advanced parameter-space-partitioning-based probabilistic analysis is illustrated in Section 5. Finally, in Section 6 the overall methodology is applied to the IEEE 69 bus and IEEE 85 test grids penetrated by PV injection.

2. Background material: Three-phase power flow analysis

We refer to a three-phase power distribution grid made of N_b buses and $N = 3 \times N_b$ nodes. Power Flow Analysis consists in the following set of nonlinear equations in the complex field:

$$\mathbf{f}_\nu(\vec{\mathbf{V}}) = \mathbf{V}_\nu^* \mathbf{I}_\nu - \mathbf{S}_\nu^* = \mathbf{0} \tag{1}$$

for $\nu = 1, \dots, N$, where $\mathbf{V}_\nu$, are voltage phasors at node ν, $\mathbf{I}_\nu$ are current phasors at node ν, and vector $\vec{\mathbf{V}} = [\mathbf{V}_1, \dots, \mathbf{V}_N]$ assembles all voltages. Complex power injected in the grid at node ν is denoted as $\mathbf{S}_\nu = P_\nu + jQ_\nu$, where P_ν and Q_ν are active and reactive power, respectively. Node currents are written as a function of node voltages via the following:

$$\mathbf{I}_\nu = \sum_{s=1}^{N} \mathbf{Y}_{\nu s} \mathbf{V}_s \tag{2}$$

where $\mathbf{Y}_{\nu s}$ are the elements of node admittance matrix [16].

In this paper, complex node voltages and currents are described in Cartesian coordinates, similarly the power flow problem Eqs. (1) are broken into their real and imaginary parts. These equations collected for all nodes $\nu = 1, \dots, N$, form a system of $2 \times N$ nonlinear real equations that can be denoted in compact form as:

$$F(\vec{V}) = 0 \tag{3}$$

where $\vec{V} = [V_1^R, V_1^I, \dots, V_N^R, V_N^I]^T$ is the column vector collecting node voltages real and imaginary parts. Such a nonlinear system can be solved with the Newton–Rapshon (NR) method that entails computing the Jacobian matrix

$$\frac{\partial F(\vec{V})}{\partial \vec{V}}. \tag{4}$$

3. Complex voltage unbalance factor

To model the potential effects that PV penetration can have on voltage unbalance, we suppose that D single-phase PV sources delivering active powers P_d, with $d = 1, \dots, D$, are injected into D *actor nodes* in the grid. This general approach covers the case where some of the injecting nodes belong to the same Bus as well as the opposite scenario where injecting nodes all belong to different Buses in the grid. Due to the uncertainty of renewable power generation, power P_d are described as continuous random variables ranging from zero to the maximum installed power P_d^M in that node. Since maximum installed powers can vary at different nodes, injected powers are mapped to normalized values:

$$x_d = \frac{P_d}{P_d^M}, \tag{5}$$

representing the *input statistical parameters* of the mathematical problem.

When the variability of PV normalized injected powers (and thus of related $P_d = x_d\, P_d^M$ powers) is included in the analysis, the power flow balance (3) can be rewritten as:

$$F(\vec{V}, \vec{x}) = 0, \tag{6}$$

where $\vec{x} = [x_1, \dots, x_D]^T$ collects statistical parameters.

To analyze voltage unbalance at nth Bus in the grid, we refer to the complex Voltage Unbalance Factor (VUF) defined as:

$$\mathbf{VUF}_n = \frac{\mathbf{V}_n^a + \mathbf{z}^2\, \mathbf{V}_n^b + \mathbf{z}\, \mathbf{V}_n^c}{\mathbf{V}_n^a + \mathbf{z}\, \mathbf{V}_n^b + \mathbf{z}^2\, \mathbf{V}_n^c}, \tag{7}$$

where $\mathbf{V}_n^a$, $\mathbf{V}_n^b$, $\mathbf{V}_n^c$ are the voltage complex phasors measured at phase a, b and c, respectively, and $\mathbf{z} = \exp j\, 120^o$.

We want to calculate the complex VUF at a subset of *observation Buses*, i.e., $\mathbf{VUF}_n$, with $n = 1, \dots, M$ in the grid, as a function of PV power injections at actor nodes. To this aim, we observe that for a given value $\vec{x}$ of normalized power parameters vector, the solution of (6) provides the associated three-phase $\vec{V}$ node voltage values that once substituted in (7) yields VUF. Voltage unbalance at nth Bus can thus be seen as a multi-variate deterministic function $\varphi_n(\cdot)$ of D normalized powers, i.e.:

$$\mathbf{VUF}_n = \varphi_n(\vec{x}). \tag{8}$$

Similarly, the vector of $\overrightarrow{VUF} = [\mathbf{VUF}_1, \dots, \mathbf{VUF}_M]^T$ at all observation nodes, can be written as a multi-output function of normalized powers

$$\overrightarrow{VUF} = \varphi(\vec{x}), \tag{9}$$

with $\varphi(\vec{x}) = [\varphi_1(\vec{x}), \dots, \varphi_M(\vec{x})]^T$.

For a given three-phase power distribution grid topology with prescribed loads, the amount of VUF determined by PV penetration strongly depends on the grid nodes where power is injected. In addition, VUF value can vary substantially at different observation Buses. This is why network operators are greatly interested in simulation tools having the following capabilities/features:

1. Simulations should identify which Buses are potentially more prone to exhibit high VUF values and they should identify which injection nodes may lead to the worst voltage unbalance conditions.
2. To investigate the worst case scenarios identified at previous point (1), accurate yet numerically-efficient probabilistic analyses are highly desirable. Such probabilistic tools should be extremely fast in order to allow exploration of several critical scenarios, be able to handle the case with many injection sources and provide detailed information about VUF probability distribution and variability intervals.

In the next Section 4, we cover the first point about VUF sensitivity, while the advanced probabilistic analysis method proposed in this paper is illustrated in Section 5.

4. Determining VUF most sensitive buses and critical PV injection nodes

The literature presents several approaches for voltage sensitivity analysis that is for computing the sensitivity of grid *node voltages* (e.g., described as real and imaginary parts) versus the assumed input parameters.

In fact, for given values of the parameters vector $\vec{x}$, voltage sensitivities can be directly derived from the solution of the power flow problem (6). It implies solving the following variational problem:

$$\frac{\partial F}{\partial \vec{V}} \cdot \frac{\partial \vec{V}}{\partial \vec{x}} = -\frac{\partial F}{\partial \vec{x}}, \tag{10}$$

where $\frac{\partial \vec{V}}{\partial \vec{x}} = [\frac{\partial V_1^R}{\partial x_d}, \frac{\partial V_1^I}{\partial x_d}, \ldots, \frac{\partial V_N^R}{\partial x_d}, \frac{\partial V_N^I}{\partial x_d}]^T$ denotes the $2N \times D$ sensitivity matrix assembling the unknown derivatives of node voltages real and imaginary parts versus parameters. The right-hand-side matrix $-\frac{\partial F}{\partial \vec{x}}$, of size $2N \times D$ too, contains the derivatives of power flow equations versus parameters. Since in our problem, input parameters are the PV-normalized active powers x_d injected at actor nodes, the dth column of matrix $-\frac{\partial F}{\partial \vec{x}}$ is a vector with a single 1 at dth actor node position and all zero the other terms. Finally, the $\frac{\partial F}{\partial \vec{V}}$ is the $2N \times 2N$ Jacobian matrix (4) employed in power flow analysis. Since, the LU decomposition of Jacobian matrix is already available from power flow solution, the solution of voltage sensitivity problem (10) requires little extra computation.

From node voltage sensitivities, it is then possible to deduce VUF sensitivity. To the aim of explaining VUF sensitivity calculation, we denote with

$$\mathbf{V}_n^a(\vec{x}) = (V_n^a)^R + j(V_n^a)^I$$
$$\mathbf{V}_n^b(\vec{x}) = (V_n^b)^R + j(V_n^b)^I$$
$$\mathbf{V}_n^c(\vec{x}) = (V_n^c)^R + j(V_n^c)^I$$

the nth Bus phase voltages, decomposed in their real and imaginary parts. Such voltages are obtained by solving the power flow problem for a given parameter vector value $\vec{x}$. Replacing such voltages into (7) gives the associated $\mathbf{VUF}_n(\vec{x})$, which reads:

$$\frac{(V_n^a)^R + j(V_n^a)^I + \mathbf{z}^2[(V_n^b)^R + j(V_n^b)^I] + \mathbf{z}[(V_n^c)^R + j(V_n^c)^I]}{(V_n^a)^R + j(V_n^a)^I + \mathbf{z}[(V_n^b)^R + j(V_n^b)^I] + \mathbf{z}^2[(V_n^c)^R + j(V_n^c)^I]}. \tag{11}$$

The computation of VUF sensitivity versus dth parameter x_d can thus be implemented analytically by applying the following chain rule derivatives:

$$\begin{aligned}\frac{\partial \mathbf{VUF}_n}{\partial x_d} = & \frac{\partial \mathbf{VUF}_n}{\partial (V_n^a)^R} \cdot \frac{\partial (V_n^a)^R}{x_d} + \frac{\partial \mathbf{VUF}_n}{\partial (V_n^a)^I} \cdot \frac{\partial (V_n^a)^I}{x_d} \\ & + \frac{\partial \mathbf{VUF}_n}{\partial (V_n^b)^R} \cdot \frac{\partial (V_n^b)^R}{x_d} + \frac{\partial \mathbf{VUF}_n}{\partial (V_n^b)^I} \cdot \frac{\partial (V_n^b)^I}{x_d} \\ & + \frac{\partial \mathbf{VUF}_n}{\partial (V_n^c)^R} \cdot \frac{\partial (V_n^c)^R}{x_d} + \frac{\partial \mathbf{VUF}_n}{\partial (V_n^c)^I} \cdot \frac{\partial (V_n^c)^I}{x_d}\end{aligned} \tag{12}$$

where:

$$\begin{aligned}&\frac{\partial \mathbf{VUF}_n}{\partial (V_n^a)^R} = \frac{D(\vec{x}) - N(\vec{x})}{D^2(\vec{x})}; \quad \frac{\partial \mathbf{VUF}_n}{\partial (V_n^a)^I} = j\frac{D(\vec{x}) - N(\vec{x})}{D^2(\vec{x})} \\ &\frac{\partial \mathbf{VUF}_n}{\partial (V_n^b)^R} = \frac{\mathbf{z}^2 D(\vec{x}) - \mathbf{z}N(\vec{x})}{D^2(\vec{x})}; \quad \frac{\partial \mathbf{VUF}_n}{\partial (V_n^b)^I} = j\frac{\mathbf{z}^2 D(\vec{x}) - \mathbf{z}N(\vec{x})}{D^2(\vec{x})} \\ &\frac{\partial \mathbf{VUF}_n}{\partial (V_n^c)^R} = \frac{\mathbf{z}D(\vec{x}) - \mathbf{z}^2 N(\vec{x})}{D^2(\vec{x})}; \quad \frac{\partial \mathbf{VUF}_n}{\partial (V_n^c)^I} = j\frac{\mathbf{z}D(\vec{x}) - \mathbf{z}^2 N(\vec{x})}{D^2(\vec{x})}\end{aligned} \tag{13}$$

while $N(\vec{x})$ and $D(\vec{x})$ denote the numerator and denominator in VUF expression, respectively, i.e.:

$$N(\vec{x}) = (V_n^a)^R + j(V_n^a)^I + \mathbf{z}^2[(V_n^b)^R + j(V_n^b)^I] + \mathbf{z}[(V_n^c)^R + j(V_n^c)^I], \tag{14}$$

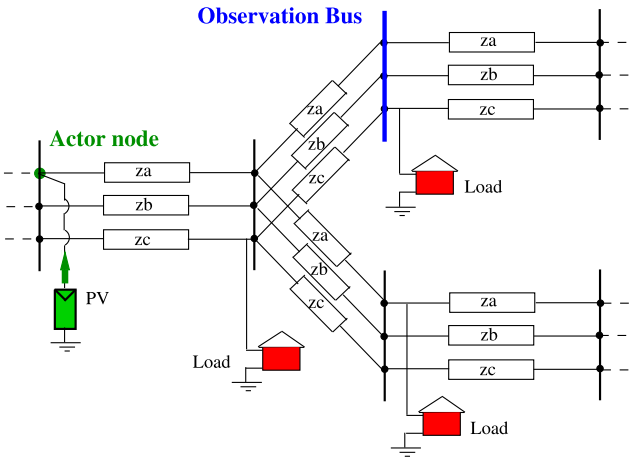

Fig. 1. Example of three-phase grid with injection at actor node j, phase a and VUF observation at Bus n.

and

$$D(\vec{x}) = (V_n^a)^R + j(V_n^a)^I + \mathbf{z}[(V_n^b)^R + j(V_n^b)^I] + \mathbf{z}^2[(V_n^c)^R + j(V_n^c)^I]. \tag{15}$$

VUF sensitivity as computed in (12), through (13), (14) and (15), is represented by a *complex number* and it is at the heart of the accelerated probabilistic analysis presented in Section 5.

However, for the purpose of determining the VUF most sensitive observation Buses in a given distribution grid and critical actor Buses, in what follows we will refer to the sensitivity modules.

In fact, we denote with:

$$s_{nj}^a = \left| \frac{\partial \mathbf{VUF}_n(\vec{x})}{\partial x_j^a} \right| \tag{16}$$

the sensitivity module of VUF at Bus of index n versus power injection at actor node at Bus of index j, phase a, as pictorially shown in Fig. 1.

Similar sensitivity coefficients s_{nj}^b and s_{nj}^c can be computed for phase b and c, respectively. However, in the hypothesis that before of PV power injection distribution grid is almost balanced, the VUF sensitivity modules versus different phase injections are almost the same, i.e. $s_{nj}^a \approx s_{nj}^b \approx s_{nj}^c$. It is thus reasonable to focus on power injection at one of the three-phase nodes, e.g., on phase a.

For a given three-phase power distribution made of N_b Buses and prescribed loads absorbing nominal powers, we can compute the VUF sensitivity modules for all Buses versus single-phase PV injection at all Buses. In this way the computed sensitivity coefficients (16) form a $N_b \times N_b$ matrix $\{s_{nj}^a\}$. We can thus introduce the following figure of merit associated to the nth observation Bus:

$$\beta_n = \sum_{j=1}^{N_b} s_{nj}^a, \tag{17}$$

that is, the sum of sensitivity modules versus all injection points. High values of such a β_n coefficient indicates which Buses in the grid are potentially more prone to exhibit large VUF. Similarly, the following figure of merit:

$$\nu_j = \sum_{n=1}^{N_b} s_{nj}^a, \tag{18}$$

indicates which Buses in the grid have actor nodes that are critical injection points.

5. Probabilistic analysis through parameter space partitioning

As already illustrated in Section 3, PV penetration in the grid is modeled by D random PV-delivered normalized powers x_d, with $d =$

$1, \dots, D$ that are collected into vector $\vec{x} = [x_1, \dots, x_D]^T$ of statistical parameters. A sufficiently wide historical data set of PV-delivered power samples, denoted as $\vec{x}^i$, with $i = 1, \dots, N_s$ (N_s is the number of samples), is exploited to perform probabilistic analysis [17].[1]

5.1. Probabilistic analysis with accelerated Monte Carlo method

Probabilistic analysis with basic Monte Carlo method implies repeating a large number of power flow simulations. In fact, for each sample of normalized power values $\vec{x}^i = [x_1, \dots, x_D]^T$, the associated PV injected power values $P_d = x_d P_d^M$ are first calculated. With these power values, the node voltages of the unbalanced three-phase grid are determined by solving the power flow analysis (3). Hence, the VUF $\mathbf{VUF}_n(\vec{x}^i)$ for the ith sample is deduced via (7). Since the numerical convergence of MC method is slow, commonly wide sample sets, with $N_s \approx 10,000$ samples or more, are needed to accurately predict VUF distribution (i.e., PDF). The computational burden grows ulteriorly when probabilistic analysis should be repeated by considering several possible injection points and many potential scenarios that can be critical for grid unbalance assessment.

Several approximate MC acceleration techniques exist that reduce the number of power flow analyses to be performed to a much smaller subset of *representative points* in the statistical parameter space. Specifically, in this paper, we focus on a a technique that identifies the important representative points in the parameter space through a data clustering method. In fact, the data clustering method illustrated in the next Subsection, allows the decomposition of parameter space into $K \ll N_s$ clusters $C_k \in \mathcal{R}^D$ having centers $\vec{c}_k$, with $k = 1, \dots, K$. Power flow analysis and related VUF complex sensitivity calculation (12) can be performed limitedly to cluster centers where are exploited to locally approximate the multi-variate functions $\mathbf{VUF}_n = \varphi_n(\vec{x})$ in (8) with the D-dimensional tangent hyperplane:

$$\varphi_n(\vec{x}) \approx \varphi_n(\vec{c}_k) + \frac{\partial \varphi_n(\vec{x})}{\partial \vec{x}}\Big|_{\vec{x}=\vec{c}_k} \cdot (\vec{x} - \vec{c}_k). \tag{19}$$

In this way, for all the samples assigned to the kth cluster, i.e., $\vec{x}^i \in C_k$, the associated VUF values $\mathbf{VUF}_n = \varphi_n(\vec{x}^i)$ can be efficiently evaluated using local approximation (19), i.e.,

$$\varphi_n(\vec{x}^i) \approx \varphi_n(\vec{c}_k) + \frac{\partial \varphi_n(\vec{x})}{\partial \vec{x}}\Big|_{\vec{x}=\vec{c}_k} \cdot (\vec{x}^i - \vec{c}_k). \tag{20}$$

5.2. Space partitioning via data clustering

Suppose that N_s samples of the normalized powers $\vec{x}^i$ are available from measurements or historical data set, we want to partition such samples into K clusters represented by centers $\vec{c}_k$, for $k = 1, \dots, K$. This goal can be achieved using a K-means clustering technique [20]. The idea behind such a technique is that a cluster can be thought of as a subset of data points whose inter-point distances are small compared with the distances to points outside of the cluster. Data partitioning consists in finding an assignment of samples to clusters, along with a set of cluster centers $\{\vec{c}_k\}$, such that the sum of the squares of the distances of each sample to its closest $\vec{c}_k$ is minimum. To formalize the assignment of samples to clusters, a set of binary indicators are introduced. For each sample $\vec{x}^i$, the binary indicators $b_{ik} \in \{0, 1\}$, with $k = 1, \dots, K$ are $b_{ik} = 1$ if sample $\vec{x}^i$ is assigned to cluster k, while $b_{ij} = 0$ for $j \neq k$. After that, the following objective function can be defined:

$$E = \sum_{i=1}^{N_s} \sum_{k=1}^{K} b_{ik} \|\vec{x}^i - \vec{c}_k\|^2 \tag{21}$$

The goal is to find values for the binary indicators $\{b_{ik}\}$ and the centers $\{\vec{c}_k\}$ that minimize E. Starting from guessing initial values for the centers, minimization is achieved via an iterative procedure that at each iteration involves two steps. In the first step, using the current values of centers, each data sample $\vec{x}^i$ is assigned to the closest cluster, i.e.

$$b_{ik} = \begin{cases} 1 & \text{if } k = \arg\min_j \|\vec{x}^i - \vec{c}_j\|^2 \\ 0 & \text{otherwise.} \end{cases} \tag{22}$$

At the second step, using the currently-computed binary indicators, the values of centers are updated as follows:

$$\vec{c}_k = \frac{\sum_{i=1}^{N_s} b_{ik} \vec{x}^i}{\sum_{i=1}^{N_s} b_{ik}}. \tag{23}$$

The two steps of re-assigning data samples to clusters and re-computing the cluster centers are repeated until there is no further change in the assignments (or until some maximum number of iterations is exceeded). Because each step reduces the value of the objective function E, convergence of the algorithm is guaranteed [20].

As an example, Fig. 2 shows the scattered plot of the samples for two (normalized) PV-delivered powers, referred to as x_1 and x_2, taken by the data set [17]. In this example, data samples are partitioned into $K = 5$ clusters each one having its own center vector $\vec{c}_k$. In this way, the parameters space is decomposed into a set of K subspace regions. It is worth observing how for a given set of N_s samples, several heuristics exist for fixing a proper number K of clusters. An approach we found effective for PV data exploits the information about the number n_k of samples assigned to the kth cluster, i.e.

$$n_k = \sum_{i=1}^{N_s} b_{ik}. \tag{24}$$

Starting from a tentative initial value, the cluster number K adopted in the k-means algorithm is gradually increased till it results that one cluster contains a too small fraction of the N_s samples, i.e. when the fraction of samples n_k/N_s in the smallest cluster goes below a given threshold (e.g., 2%).

We end this Section by summarizing in Fig. 3 the main computational steps of the accelerated probabilistic MC analysis derived from K-means space-partitioning. It is worth noticing how the computational cost is largely dominated by the solution of the K Load Flow problems

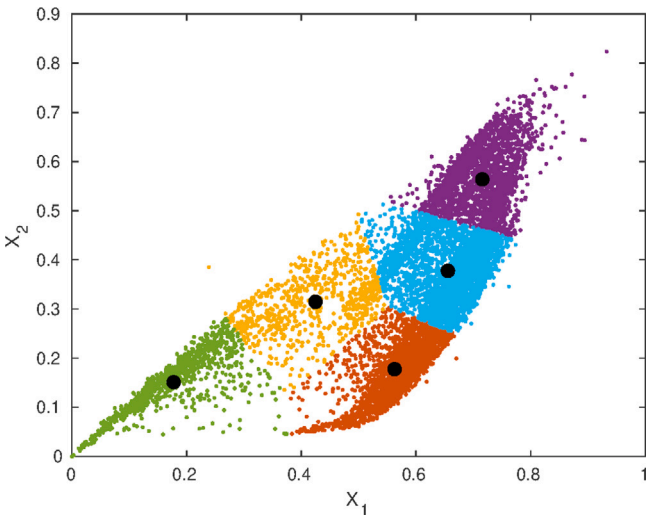

Fig. 2. Example of data clustering with $K = 5$ number of clusters. Filled black circles indicate the cluster centers $\vec{c}_k$, points with the same color indicate the samples belonging to the same cluster. (For interpretation of the references to color in this figure legend, the reader is referred to the web version of this article.)

[1] In the case available data samples is not wide enough, repopulation techniques can be employed to generate new samples [18,19].

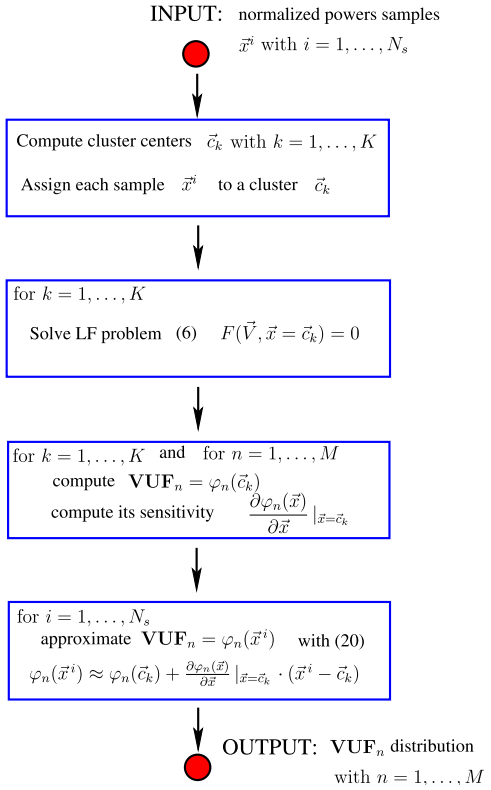

Fig. 3. Computational Flow Chart of the K-means space-partitioning accelerated MC.

at the centers of the clusters while subsequent VUF and sensitivity computations require little extra computation.

6. Numerical results and experiments

In this Section, we investigate voltage unbalance caused by PV penetration in modified three-phase versions of the IEEE 69 bus and IEEE 85 bus test cases supplied in the MatPower software suite [21]. More specifically, in Section 6.1 we apply sensitivity analysis method to identify the VUF most critical buses in the radial IEEE 69 grid. In subsequent Section 6.2, the space-partitioning accelerated MC is employed to perform probabilistic analysis of the PV penetrated IEEE 69 grid subject to balanced and unbalanced PV injection. Finally, Section 6.3 illustrates the portability of the proposed analysis method to more general scenarios. In fact, in this last example sensitivity and probabilistic analysis are applied to a configurable IEEE 85 bus grid that can work either as radial or meshed topology. Numerical simulations have been done using the Matlab code described in [22]. The machine used is an Intel I7 with 16 GB of ram and 2.3 GHz clock frequency.

6.1. VUF sensitivity analysis

Grid topology of IEEE 69 bus network and related buses numbering are shown in Fig. 4. In our simulations, the single-phase IEEE 69 bus grid is extended to a three-phase grid by duplicating the assigned single-phase loads (i.e., their active and reactive powers) at the three-phase nodes of each bus. In the three-phase IEEE 69 bus grid, the total active power absorbed by loads is of $P = 11.4$ MW.

Starting from the three-phase grid in balanced condition, i.e., $\vec{x} = \vec{0}$, VUF sensitivity versus single-phase PV power injection is calculated according to the method illustrated in Section 4.

In particular, complex VUF sensitivity for all Buses versus all injection nodes is calculated. As an instance of such a calculation,

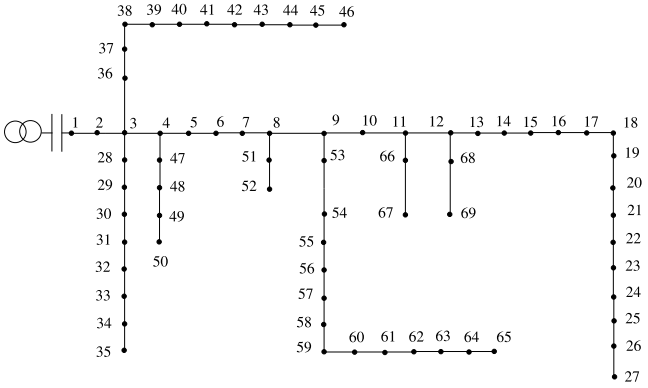

Fig. 4. The IEEE 69 bus radial distribution grid.

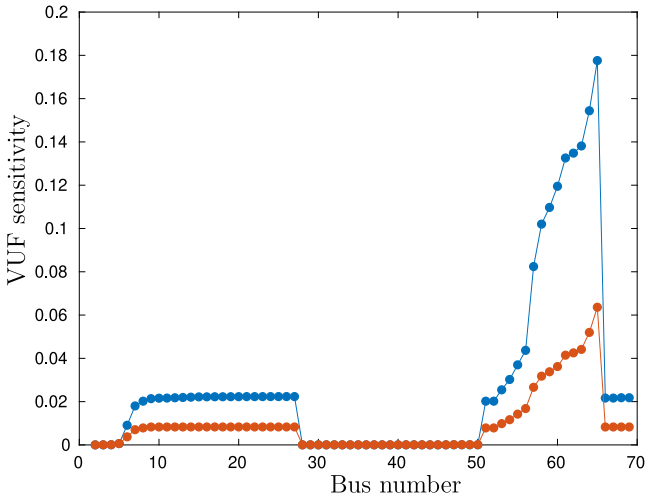

Fig. 5. (Blue) Real and (Red) imaginary parts of complex VUF sensitivities $\frac{\partial \mathbf{VUF}_{65}(\vec{0})}{\partial x_j^a}$ for $j = 1, \dots, 69$, phase a. (For interpretation of the references to color in this figure legend, the reader is referred to the web version of this article.)

Fig. 5 shows the real and imaginary parts of complex VUF sensitivities $\frac{\partial \mathbf{VUF}_n(\vec{0})}{\partial x_j^a}$ for Bus $n = 65$ versus injection at all Buses $j = 1, \dots, 69$, phase a.

It is seen how VUF observed at node 65 is highly sensitive to single-phase power injection at the nearby Buses in the same feeder (e.g., $j = 59, \dots, 65$) with a maximum just at Bus $j = 65$.

Fig. 6, instead, reports the complex VUF sensitivities

$$\mathbf{s}_{nj}^a = \frac{\partial \mathbf{VUF}_n(\vec{0})}{\partial x_j^a}, \quad \mathbf{s}_{nj}^b = \frac{\partial \mathbf{VUF}_n(\vec{0})}{\partial x_j^b}, \quad \mathbf{s}_{nj}^c = \frac{\partial \mathbf{VUF}_n(\vec{0})}{\partial x_j^c} \tag{25}$$

for Bus $n = 65$ versus the three phases a, b and c at Bus $j = 60$.

It is seen how the three complex sensitivities are balanced, i.e. they have the same modules and relative phase differences of 120°, and thus $\mathbf{s}_{nj}^a + \mathbf{s}_{nj}^b + \mathbf{s}_{nj}^c = \mathbf{0}$. This result is correct since sensitivities have been calculated for a three-phase power grid operating in balanced conditions. In such a condition, PV power injections Δx_j^a, Δx_j^b and Δx_j^c at the three phases of Bus j produce a complex VUF variation at observation node n that reads:

$$\Delta \mathbf{VUF}_n = \mathbf{s}_{nj}^a \cdot \Delta x_j^a + \mathbf{s}_{nj}^b \cdot \Delta x_j^b + \mathbf{s}_{nj}^c \cdot \Delta x_j^c. \tag{26}$$

If power injections at the three phases are the same, i.e., $\Delta x_j^a = \Delta x_j^b = \Delta x_j^c = \Delta x$, the grid remains balanced and the resulting voltage unbalance $\Delta \mathbf{VUF}_n$ is zero, as correctly predicted by complex-domain model (26).

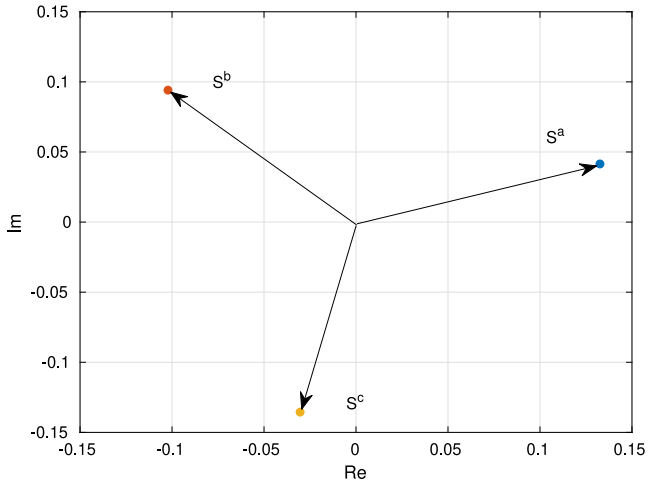

Fig. 6. Complex VUF sensitivities for Bus $n = 65$ versus injection at the three phases a, b and c at nearby Bus $j = 60$. Complex sensitivities are balanced, i.e. $\mathbf{s}^a + \mathbf{s}^b + \mathbf{s}^c = \mathbf{0}$.

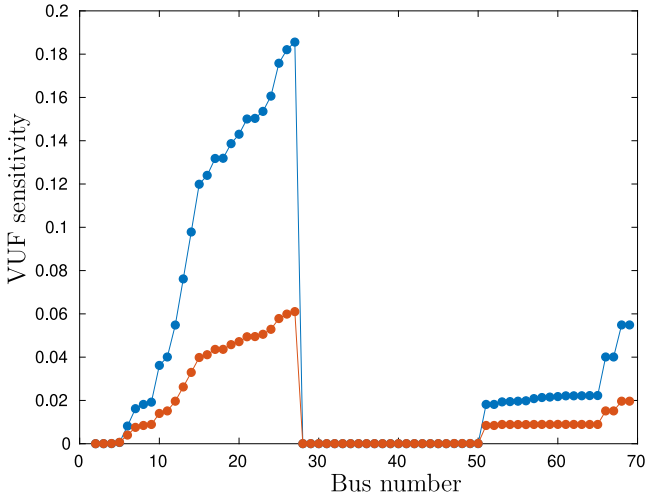

Fig. 7. (Blue) Real and (Red) imaginary parts of complex VUF sensitivities $\frac{\partial \mathbf{VUF}_{27}(\vec{0})}{\partial x_j^a}$ for $j = 1, \dots, 69$, phase a. (For interpretation of the references to color in this figure legend, the reader is referred to the web version of this article.)

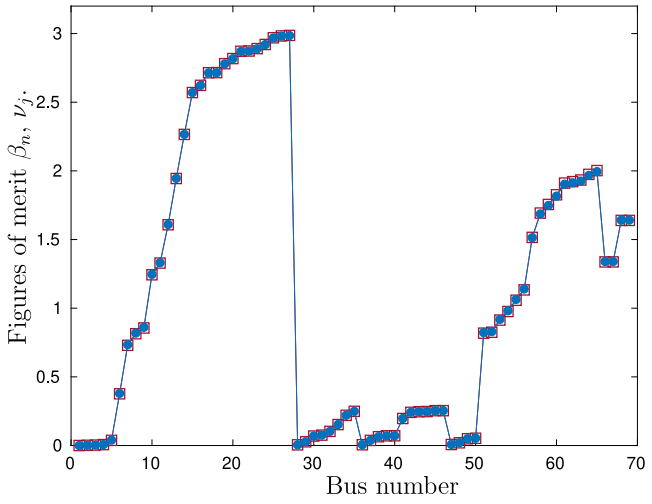

Fig. 8. (Dot Marker) figure of merit β_n, (Square Marker) figure of merit ν_j.

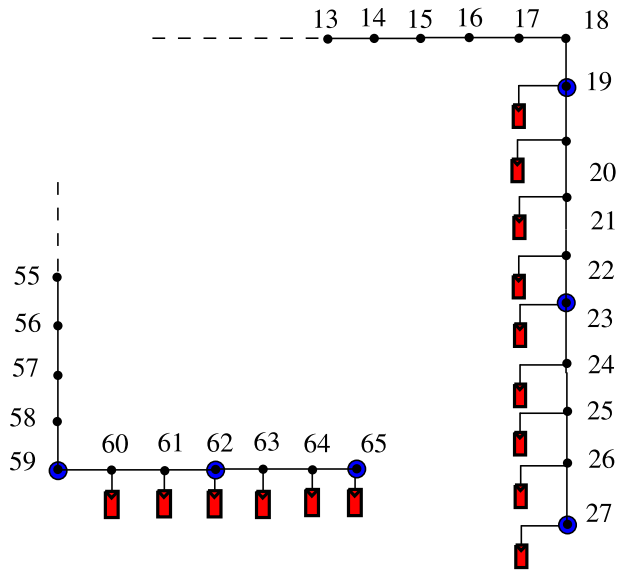

Fig. 9. Unbalanced injection of PV sources. All sources are connected to Phase-A nodes. PV injection buses are indicated with a red box, blue dots denote VUF observation buses.

As a second instance, Fig. 7 shows the real and imaginary parts of complex VUF sensitivities calculated for Bus $n = 27$ versus at all Buses $j = 1, \dots, 69$, phase a.

Also, in this case, VUF at node 27 is highly sensitive to single-phase power injection at Buses in the same feeder (e.g., $j = 19, \dots, 27$) with a maximum just at $j = 27$.

After that, in order to identify the VUF most critical Buses in the grid, we focus on VUF sensitivities modules and calculate the figures of merit β_n and ν_j as defined in (17) and (18).

Fig. 8 reports the coefficient values: it is seen how Buses with indices $n = 19, \dots, 27$ have the highest β_n values. These Buses are thus potentially the most prone to exhibit large VUF values due to single-phase power injection. Other Buses with relatively high β_n values are those numbered with indices $n = 59, \dots, 65$. It is worth noting how the second figure of merit ν_j follows the first one, i.e., $\beta_k \approx \nu_k$. This means that the most critical VUF observation Buses are also the most critical power injection points. By exploiting the clear insights that preliminary VUF sensitivity analysis can provide for the grid under test, it is now possible to identify a small set of critical scenarios that are worth simulating with probabilistic methods in order to assess grid unbalance performance.

6.2. Probabilistic analysis of critical scenario

As an example, we provide analysis results for the unbalanced-injection critical scenario where 15 PV power sources are connected to Buses with numbers $j = 60, \dots, 65$ and $j = 19, \dots, 27$, as shown in Fig. 9. The selected PV injection nodes are suggested by previously presented VUF sensitivity analysis. In all of such Buses, power injection is done into single Phase-A node. Such an unbalanced PV injection arrangement corresponds to the critical scenario.

Each power source represents the aggregation of many PV plants and corresponds to a maximum installed PV power of $P_d^M = 300$ kW. The samples of normalized power delivery x_d, for $d = 1, \dots, 15$ are extracted from the historic data set [17]. According to (5), normalized powers are scaled by the assumed maximum installed power to provide actual PV power values $P_d = x_d \cdot P_d^M$ to be used in simulations. Since, in IEEE 69 bus test case, the total active power absorbed by loads is of $P = 11.4$ MW, the total installed PV power of $300\,\text{kW} \times 15 = 4.5$ MW corresponds to a PV penetration of $\alpha = 4.5/11.4 \approx 40\%$. We

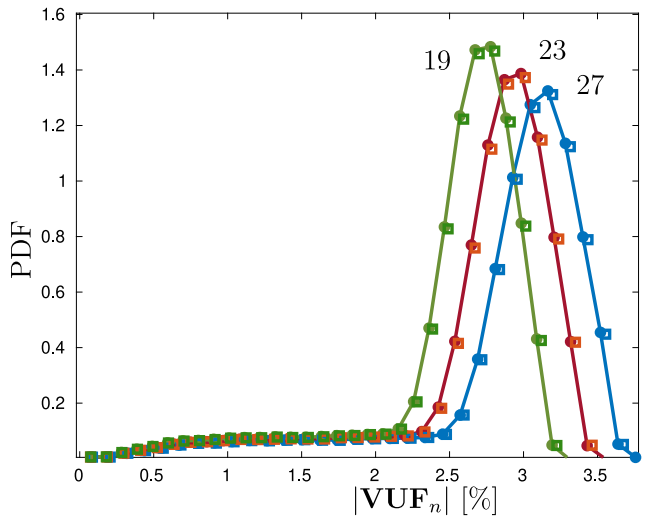

Fig. 10. Unbalanced injection scenario. PDF($|\mathbf{VUF}_n|$) at Buses: (Blue line) $n = 27$; (Red line) $n = 23$; (Green line) $n = 19$ computed with the space-partitioning-accelerated MC. The Square markers, (Blue, Red and Green) indicate the respective PDFs as computed with reference MC (10,000 simulations). (For interpretation of the references to color in this figure legend, the reader is referred to the web version of this article.)

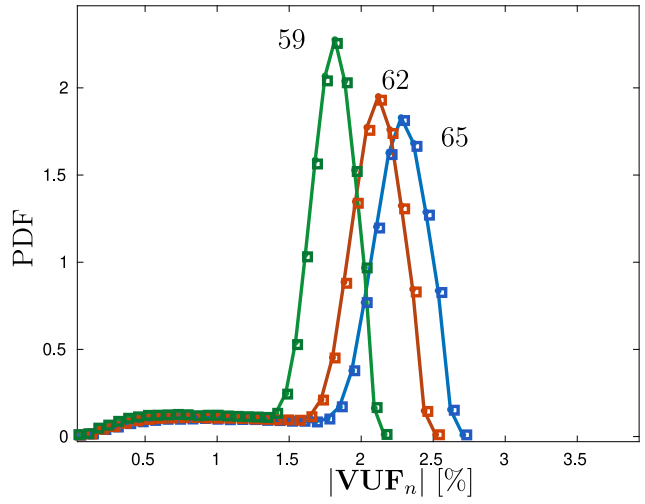

Fig. 11. Unbalanced injection scenario. PDF($|\mathbf{VUF}_n|$) at Buses: (Blue line) $n = 65$; (Red line) $n = 62$; (Green line) $n = 59$ computed with the space-partitioning-accelerated MC. The Square markers, (Blue, Red and Green) indicate the respective PDFs as computed with reference MC (10,000 simulations). (For interpretation of the references to color in this figure legend, the reader is referred to the web version of this article.)

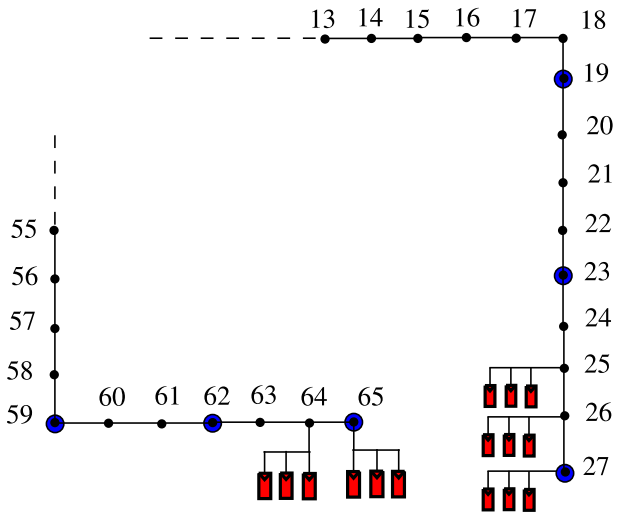

Fig. 12. Balanced injection of PV sources: sources are applied to the three-phase nodes. PV injection buses are indicated with a triplet of red boxes, while blue dots denote VUF observation buses. (For interpretation of the references to color in this figure legend, the reader is referred to the web version of this article.)

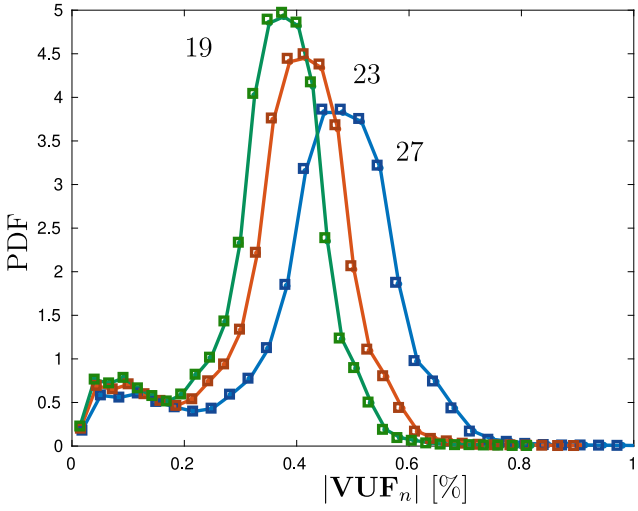

Fig. 13. Balanced injection scenario. PDF($|\mathbf{VUF}_n|$) at Buses: (Blue line) $n = 27$; (Red line) $n = 23$; (Green line) $n = 19$ computed with the space-partitioning-accelerated MC. The Square markers, (Blue, Red and Green) indicate the respective PDFs as computed with reference MC (10,000 simulations). (For interpretation of the references to color in this figure legend, the reader is referred to the web version of this article.)

perform probabilistic analysis with the space-partitioning-accelerated MC method presented in Section 5, samples data are partitioned into $K = 11$ clusters. Results are compared with those provided by reference MC method running 10,000 load flow simulations. Fig. 10 reports the PDFs of the VUF module (in %) at the three Buses $n = 19, 23, 27$ in the right-most feeder. It is seen how voltage unbalance variability interval is larger at the feeder-ending Bus $n = 27$ where VUF module has a nonzero probability of reaching the 3.5% value. In this unbalanced PV injection scenario, and for the assumed $\alpha \approx 40\%$ penetration level, the VUF module at the three Buses $n = 19, 23, 27$ has a $\approx 95\%$ probability of exceeding the safety threshold of 2%.

Similarly, Fig. 11 shows the PDFs of the VUF module at the three Buses $n = 59, 62, 65$ in the left feeder. Also in this case the feeder largest voltage unbalance variability interval is achieved at the ending Bus $n = 65$ where VUF module has a nonzero probability of reaching the 2.5% value. As it was correctly predicted by VUF sensitivity analysis, left feeder is less critical than right one in terms of VUF.

Hence, we pass to consider a second PV injection scenario where the 15 PV sources are connected to all the three-phase nodes of the Buses with numbers $j = 64, 65$ and $j = 25, 26, 27$, as shown in Fig. 12.

We refer to such an arrangement to as the balanced-injection scenario even though it is worth noticing how the PV sources connected to the three phases of the same Bus are represented by different random variables whose samples are extracted from the historical data set. As in the critical scenario, the maximum installed power for each source is $P_d^M = 300$ kW and the grid PV penetration is $\alpha \approx 40\%$.

Fig. 13 reports the PDFs of the VUF module (in %) at the three Buses $n = 19, 23, 27$ in the right-most feeder for the balanced injection scenario. When compared to unbalanced injection case shown in Fig. 10, it is seen a remarkable reduction of VUF variability interval that, for the critical observation Bus 27 has zero probability of exceeding the 0.8%

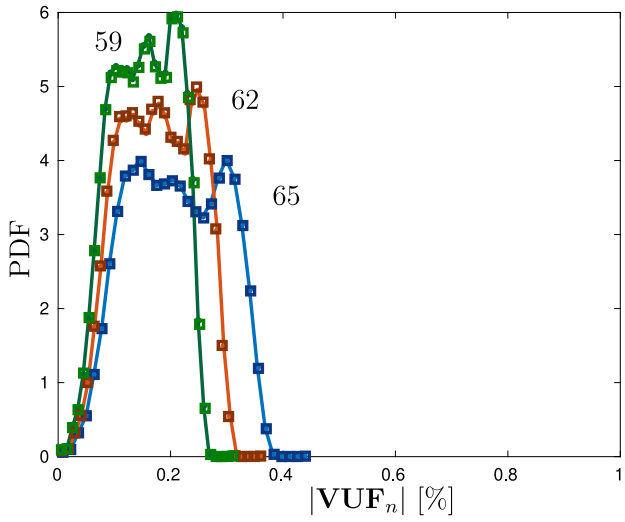

Fig. 14. Balanced injection scenario. PDF($|\mathbf{VUF}_n|$) at Buses: (Blue line) $n = 65$; (Red line) $n = 62$; (Green line) $n = 59$ computed with the space-partitioning-accelerated MC. The Square markers, (Blue, Red and Green) indicate the respective PDFs as computed with reference MC (10,000 simulations). (For interpretation of the references to color in this figure legend, the reader is referred to the web version of this article.)

Table 1
Methods comparison: IEEE 69 Bus ($D = 15$ parameters).

	Numb. LF sim.	Sim. time [s]	Relative error
Reference MC	10,000	423	–
Accelerated MC	11	0.9	$< 0.5\%$
gPC	136	11	$< 0.5\%$

value. A similar conclusion holds for VUF at the left feeder, as shown in Fig. 14, where VUF variability interval is predicted to be $< 0.5\%$.

The correctness of such results have been confirmed by simulations with reference MC method (running 10,000 repeated Load Flow simulations). From Figs. 10, 11, 13, and 14 we see that the results obtained with space-partitioning-accelerated MC method match with excellent accuracy those provided by reference MC method. Table 1 reports the comparison between the two methods in terms of number of required Load Flow analyses, overall simulation time and relative error introduced by the proposed acceleration technique (checked in all of the Buses in the grid).

As a further verification, we compare the proposed space-partitioning-accelerated MC method with the state-of-the-art MC acceleration technique based on generalized Polynomial Chaos (gPC) surrogate model [11,23–25]. We remind here that for D statistical parameters and approximation order γ, the gPC method requires performing at least

$$\frac{(D+\gamma)!}{D!\,\gamma!} \tag{27}$$

repeated Load Flow simulations. Hence, for $D = 15$ parameters and approximation order $\gamma = 2$, the gPC method requires ≥ 136 Load Flow simulations. Comparison with the evaluation indices of gPC method, as reported in Table 1, shows that the proposed space-partitioning-accelerated MC introduces an $\approx 10\times$ speed-up factor over gPC method, for a comparable accuracy.

6.3. Method extension

In this final subsection, we illustrate a further numerical example that shows how the proposed sensitivity analysis and advanced probabilistic method are portable and scalable to more complex scenarios. To this aim we consider the IEEE 85 bus grid reported in Fig. 15. Such a

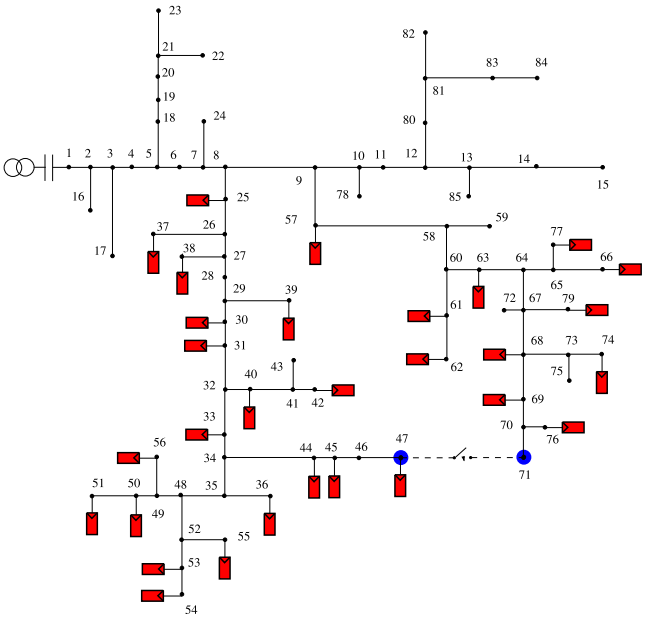

Fig. 15. The reconfigurable IEEE 85 bus grid; the branch (dashed line) connecting Bus 47 and Bus 71 can be switched-on to form a ring.

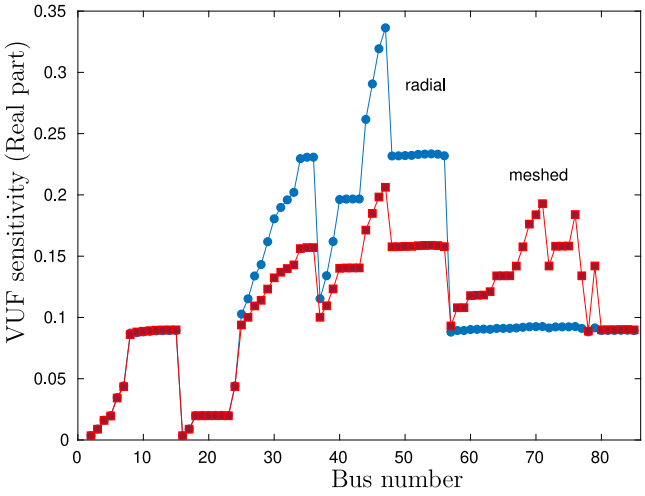

Fig. 16. Real parts of complex VUF sensitivities computed at Bus 47 in the: (Blue line) radial and (Red line) meshed configurations. (For interpretation of the references to color in this figure legend, the reader is referred to the web version of this article.)

network can be reconfigured in a weakly meshed grid by switching-on the branch (shown in the figure with a dashed line) connecting Bus 47 with Bus 71.

Complex VUF sensitivity for all Buses versus all injection nodes can be efficiently calculated with the proposed technique. For instance, Fig. 16 reports the real parts of complex VUF sensitivities $\frac{\partial \mathbf{VUF}_n(\vec{0})}{\partial x_j^a}$ for Bus $n = 47$ versus injection at all Buses $j = 1, \ldots, 85$, phase a, as computed in the radial and meshed grid configurations. It is seen how for the radial grid, VUF sensitivity sharply depends on power injection at nearby Buses in the same feeder. By contrast, in the meshed grid, sensitivity is reduced in value and almost uniform with respect to the Buses forming the mesh. Similar considerations hold for the imaginary parts of complex VUF sensitivities, as shown in Fig. 17.

The probabilistic analysis of IEEE 85 bus grid can be performed efficiently with the accelerated MC method allowing the exploration of several critical scenarios. As a numerical example, in what follows,

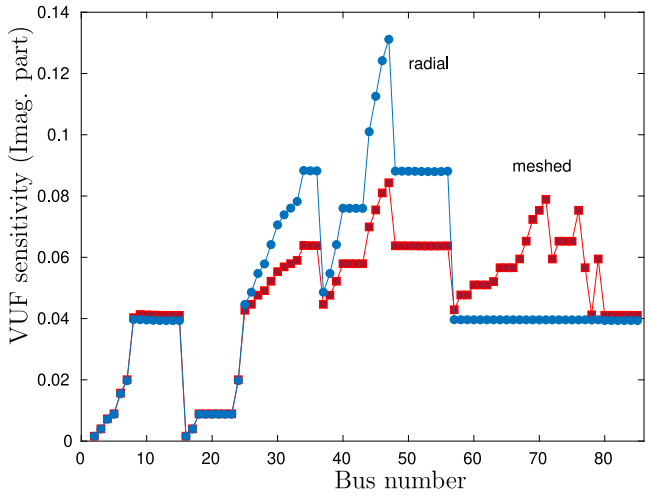

Fig. 17. Imaginary parts of complex VUF sensitivities computed at Bus 47 in the: (Blue line) radial and (Red line) meshed configurations. (For interpretation of the references to color in this figure legend, the reader is referred to the web version of this article.)

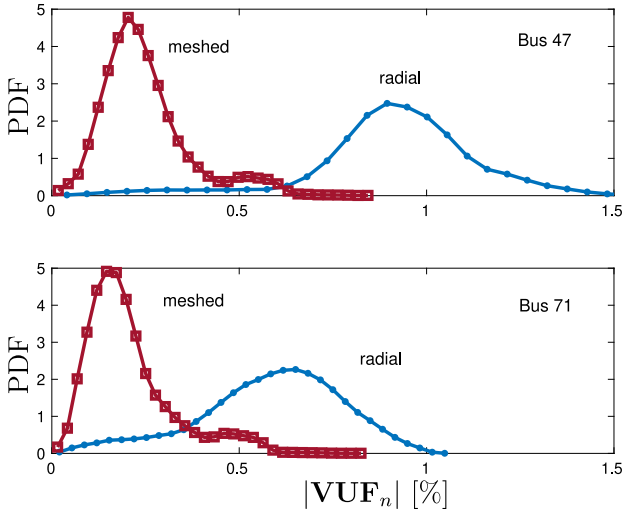

Fig. 18. PDF($|\mathbf{VUF}_n|$) at Buses $n = 47$ and $n = 71$ computed for the cases: (Blue line) radial grid; (Red line) meshed grid. (For interpretation of the references to color in this figure legend, the reader is referred to the web version of this article.)

we present results for the case where $D = 30$ single-phase PV power sources, each one injecting a maximum installed PV power of $P_d^M = 300$ kW, are connected to the Buses highlighted in Fig. 15. In this simulation case, the 30 PV sources are equally distributed among the three phases, i.e., 10 sources (randomly selected) are injected at Phase-A, 10 at Phase-B and 10 at Phase-C node of related Buses.

In this case, having $D = 30$ input variables, data samples are partitioned into $K = 16$ clusters using the K-means method outlined in Section 5.2. Probabilistic analysis is thus performed with the space-partitioning accelerated MC and results are compared with those provided by the reference MC method and by gPC-based acceleration method.

Fig. 18 reports the PDFs of the VUF module (in %) at the observable Buses $n = 47$ and $n = 71$ for the radial and meshed grid. It is clearly seen how the meshed topology results in a significant reduction of the VUF variability interval for both buses $n = 47$ and $n = 71$.

Finally, Table 2 reports the comparison among the methods: in this second grid having $D = 30$ input statistical parameters the computational speed-up introduced by space-partitioning-method over gPC method grows to $\approx 25\times$.

Table 2
Methods comparison: IEEE 85 Bus ($D = 30$ parameters).

	Numb. LF sim.	Sim. time [s]	Relative error
Reference MC	10,000	441	–
Accelerated MC	16	1.3	$< 0.5\%$
gPC	496	37	$< 0.5\%$

7. Discussion and conclusion

This paper has presented some advanced computational tools for the evaluation of Voltage Unbalance Factor (VUF) in PV penetrated three-phase distribution grids. The challenges connected with such an issue are many and include the complex and non-elementary expression of the VUF quantity, the great variability it can exhibit at different observation buses in the grid as well as its dependence on the many potential nodes where PV powers could be injected. In addition to that, PV delivered powers are uncertain, commonly described by non-standard (e.g., non-Normal) statistical distributions that are deduced from historic data sets.

The method presented in this paper relies on the definition (7) of complex VUF and on the computation of its sensitivity versus all the potential injection points in the grid, as it has been illustrated in Section 4. In the Numerical experiments shown in Fig. 6 and example given by (26), it has been highlighted how the complex-domain modeling of VUF is indeed indispensable in order to correctly compose together the effects of power injection at different phases. Complex VUF sensitivities allows one to build accurate local multi-variate approximations (19) of VUF-versus-injected powers relationship at different locations in the statistical space. On the other hand, it has been described how the modules of VUF sensitivities, as given in (16), allow one to identify key figures of merit (17) and (18) that clearly suggest which are the most critical observation feeders and Buses in the grid and the critical PV injection scenarios. Finally, an advanced probabilistic analysis method has been presented that is able to handle in a numerically efficient, yet accurate way, grids penetrated by many PV sources which are described by large data set of historic samples. The novel method proposed overcomes the curse of dimensionality problem by decomposing the multi-variate statistical space into small subspace regions via a data clustering method. It has been shown how such a space-partitioning method combined with local multi-variate approximations (19) of VUF-versus-injected powers can provide dramatic accelerations of MC-based probabilistic analysis. For the IEEE 69 bus and IEEE 85 bus test grids herein considered, a more than two orders of magnitude simulation speed-up is introduced compared to reference MC method for a comparable accuracy. Space-partitioning method introduces a significant simulation speed-up also when compared to state-of-the art surrogate models based on generalized polynomial chaos methods. Such a speed-up factor grows with the number of the input statistical parameters considered in the analysis.

CRediT authorship contribution statement

Giambattista Gruosso: Supervision, Conceptualization, Methodology, Software, Validation, Writing – review & editing. **Cesar Diaz Londono:** Data curation, Writing – original draft. **Luca Daniel:** Visualization, Investigation, Conceptualization, Methodology. **Paolo Maffezzoni:** Supervision, Conceptualization, Methodology, Software, Validation, Writing – review & editing.

Declaration of competing interest

The Authors of the paper declare that haven t any con ict of interest.

Data availability

Data will be made available on request.

References

[1] Liu Z, Milanovic JV. Probabilistic estimation of voltage unbalance in MV distribution networks with unbalanced load. IEEE Trans Power Deliv 2015;30(2):693–703. http://dx.doi.org/10.1109/TPWRD.2014.2322391.

[2] von Jouanne A, Banerjee B. Assessment of voltage unbalance. IEEE Trans Power Deliv 2001;16(4):782–90. http://dx.doi.org/10.1109/61.956770.

[3] Munikoti S, Natarajan B, Jhala K, Lai K. Probabilistic voltage sensitivity analysis to quantify impact of high PV penetration on unbalanced distribution system. IEEE Trans Power Syst 2021;36(4):3080–92. http://dx.doi.org/10.1109/TPWRS.2021.3053461.

[4] Fan M, Vittal V, Heydt GT, Ayyanar R. Probabilistic power flow studies for transmission systems with photovoltaic generation using cumulants. IEEE Trans Power Syst 2012;27(4):2251–61.

[5] Mohammadi M, Shayegani A, Adaminejad H. A new approach of point estimate method for probabilistic load flow. Int J Electr Power Energy Syst 2013;51:54–60. http://dx.doi.org/10.1016/j.ijepes.2013.02.019.

[6] Usaola J. Probabilistic load flow with wind production uncertainty using cumulants and Cornish–Fisher expansion. Int J Electr Power Energy Syst 2009;31(9):474–81. http://dx.doi.org/10.1016/j.ijepes.2009.02.003, Power Systems Computation Conference (PSCC) 2008.

[7] Hajian M, Rosehart WD, Zareipour H. Probabilistic power flow by Monte Carlo simulation with Latin supercube sampling. IEEE Trans Power Syst 2013;28(2):1150–9.

[8] Xie ZQ, Ji TY, Li MS, Wu QH. Quasi-Monte Carlo based probabilistic optimal power flow considering the correlation of wind speeds using copula function. IEEE Trans Power Syst 2018;33(2):2239–47. http://dx.doi.org/10.1109/TPWRS.2017.2737580.

[9] Gruosso G, Netto RS, Daniel L, Maffezzoni P. Joined probabilistic load flow and sensitivity analysis of distribution networks based on polynomial chaos method. IEEE Trans Power Syst 2020;35(1):618–27. http://dx.doi.org/10.1109/TPWRS.2019.2928674.

[10] Gruosso G, Maffezzoni P, Zhang Z, Daniel L. Probabilistic load flow methodology for distribution networks including loads uncertainty. Int J Electr Power Energy Syst 2019;106:392–400.

[11] Gruosso G, Maffezzoni P. Data-driven uncertainty analysis of distribution networks including photovoltaic generation. Int J Electr Power Energy Syst 2020;121:106043.

[12] Gruosso G, Gajani GS, Zhang Z, Daniel L, Maffezzoni P. Uncertainty-aware computational tools for power distribution networks including electrical vehicle charging and load profiles. IEEE Access 2019;7:9357–67.

[13] Pillay P, Manyage M. California electricity situation. IEEE Power Eng Rev 2001;21(5):10–2. http://dx.doi.org/10.1109/39.920965.

[14] Yan R, Saha TK. Voltage variation sensitivity analysis for unbalanced distribution networks due to photovoltaic power fluctuations. IEEE Trans Power Syst 2012;27(2):1078–89. http://dx.doi.org/10.1109/TPWRS.2011.2179567.

[15] Valverde G, Van Cutsem T. Model predictive control of voltages in active distribution networks. IEEE Trans Smart Grid 2013;4(4):2152–61. http://dx.doi.org/10.1109/TSG.2013.2246199.

[16] Powell L. Power System Load Flow Analysis. Electrical engineering, Mcgraw-hill; 2004, URL https://books.google.it/books?id=2B2RZZcLMwwC.

[17] DKA Solar Centre, Alice Springs Project. URL https://dkasolarcentre.com.au/.

[18] Widén J, Shepero M, Munkhammar J. Probabilistic load flow for power grids with high PV penetrations using copula-based modeling of spatially correlated solar irradiance. IEEE J Photovolt 2017;7(6):1740–5.

[19] Palahalli H, Maffezzoni P, Arboleya P, Gruosso G. Implementing stochastic response surface method and Copula in the presence of data-driven PV source models. IEEE Trans Sustain Energy 2022;13(4):2370–80. http://dx.doi.org/10.1109/TSTE.2022.3197893.

[20] Bishop CM. Pattern recognition and machine learning, first ed.. Springer; 2006.

[21] Das D. Optimal placement of capacitors in radial distribution system using a fuzzy-GA method. Int J Electr Power Energy Syst 2008;30(6):361–7.

[22] Maffezzoni P, Gruosso G. Complex-array-operation Newton solver for power grids simulations. IEEE Access 2020;8:47984–92. http://dx.doi.org/10.1109/ACCESS.2020.2979775.

[23] Xiu D, Karniadakis GE. The Wiener–Askey polynomial chaos for stochastic differential equations. SIAM J Sci Comput 2002;24(2):619–44.

[24] Zhang Z, Yang X, Marucci G, Maffezzoni P, Elfadel IAM, Karniadakis G, et al. Stochastic testing simulator for integrated circuits and MEMS: Hierarchical and sparse techniques. In: Proceedings of the IEEE 2014 custom integrated circuits conference. IEEE; 2014, p. 1–8.

[25] Wu H, Zhou Y, Dong S, Song Y. Probabilistic load flow based on generalized polynomial chaos. IEEE Trans Power Syst 2017;32(1):820–1. http://dx.doi.org/10.1109/TPWRS.2016.2543143.